

Local application of engineered insulin-like growth factor I mRNA demonstrates regenerative therapeutic potential *in vivo*

Justin S. Antony,¹ Pascale Birrer,¹ Claudia Bohnert,¹ Sina Zimmerli,¹ Petra Hillmann,¹ Hervé Schaffhauser,¹ Christine Hoeflich,² Andreas Hoeflich,² Ramzi Khairallah,³ Andreas T. Satoh,¹ Isabelle Kappeler,¹ Isabel Ferreira,¹ Klaas P. Zuideveld,¹ and Friedrich Metzger¹

¹Versameb AG, Technology Park, 4057 Basel, Switzerland; ²Ligandis, 18276 Gülzow-Prüzen, Germany; ³Myologica LLC, Baltimore, MD 21212, USA

Insulin-like growth factor I (IGF-I) is a growth-promoting anabolic hormone that fosters cell growth and tissue homeostasis. IGF-I deficiency is associated with several diseases, including growth disorders and neurological and musculoskeletal diseases due to impaired regeneration. Despite the vast regenerative potential of IGF-I, its unfavorable pharmacokinetic profile has prevented it from being used therapeutically. In this study, we resolved these challenges by the local administration of IGF-I mRNA, which ensures desirable homeostatic kinetics and non-systemic, local dose-dependent expression of IGF-I protein. Furthermore, IGF-I mRNA constructs were sequence engineered with heterologous signal peptides, which improved *in vitro* protein secretion (2- to 6-fold) and accelerated *in vivo* functional regeneration (16-fold) over endogenous IGF-I mRNA. The regenerative potential of engineered IGF-I mRNA was validated in a mouse myotoxic muscle injury and rabbit spinal disc herniation models. Engineered IGF-I mRNA had a half-life of 17–25 h in muscle tissue and showed dose-dependent expression of IGF-I over 2–3 days. Animal models confirm that locally administered IGF-I mRNA remained at the site of injection, contributing to the safety profile of mRNA-based treatment in regenerative medicine. In summary, we demonstrate that engineered IGF-I mRNA holds therapeutic potential with high clinical translatability in different diseases.

INTRODUCTION

Insulin-like growth factor I (IGF-I) is a growth-promoting hormone that regulates multiple physiological activities, including cell growth as well as tissue repair and regeneration.¹ The clinical significance of IGF-I has been investigated in various disease conditions, including growth disorders, diabetes, neurological diseases, cardiovascular diseases, and musculoskeletal diseases.² The role of IGF-I in muscle growth, repair, and regeneration is well understood.² IGF-I coordinates satellite cell activation and myogenesis during myogenic processes throughout muscle development, growth, and regeneration.^{3–5} Furthermore, recovery from myotoxic injury is delayed in skeletal muscle in IGF-I receptor (IGF-IR) knockout mice because of a lack

of myoblast fusion.⁶ IGF-I is a key factor in tissue repair after injury in other tissues besides muscle, such as in the spinal cord after disc herniation, but also beyond.^{7,8} Because of the critical role of IGF-I in homeostasis of regenerative tissues, the therapeutic potential of recombinant human IGF-I (rhIGF-I) has been investigated in several clinical trials, particularly in muscle and brain disorders.^{9–11}

An obstacle to IGF-I therapy that has not been overcome so far is the short half-life of the recombinant protein when applied systemically. Consequently, dosing limitations restrict its therapeutic application and clinical development to severe IGF-I deficiency. Acute side effects such as hypoglycemia and suppression of growth hormone (GH) release after subcutaneous (s.c.) application of rhIGF-I led to the development of, among other things, a polyethylene glycol (PEG)-modified IGF-I that improved systemic exposure^{12–14} and prolonged half-life, and physiological features after s.c. application in humans showed an improved safety profile.² Nevertheless, local application of PEGylated IGF-I into skeletal muscle did not provide sustained muscle levels that would be necessary to achieve major benefit for recovery from muscle injury.¹⁵ Therefore, we hypothesized that providing sustained kinetics through localized translation of mRNA coding for human IGF-I can potentially overcome the problems of single injections of rhIGF-I or PEGylated IGF-I for more persistent tissue IGF-I exposure. Earlier studies have documented the therapeutic benefit of IGF-I mRNA in myocardial infarction (MI) and osteoarthritis (OA).^{16,17}

Because of the disadvantages of high-dose whole-body exposure of rhIGF-I, local and site-specific IGF-I treatment is preferred over systemic administration.^{18,19} For local administration of mRNA, simple (“naked”) formulations can be used. Several studies have confirmed its higher efficiency compared with lipid nanoparticle (LNP) or other equivalent formulations in different tissue matrices including

Received 27 April 2023; accepted 11 October 2023;
<https://doi.org/10.1016/j.omtn.2023.102055>.

Correspondence: Justin S. Antony, Versameb AG, Hochbergerstrasse 60C, 4057 Basel, Switzerland.

E-mail: justin.a.selvaraj@versameb.com



muscles.^{20–23} The application of naked mRNA further avoids the large volumes of LNP-formulated mRNA. Therefore, naked administration represents an additional benefit for local application into volume-restricted tissue compartments such as vertebral discs or knees. To enable the local administration of very low mRNA amounts that lead to local production of therapeutic levels of IGF-I, IGF-I mRNA was optimized to minimize the dose. Additionally, the optimization reduces the risk for immunogenicity and other mRNA-related side effects.²⁴ Signal peptides (SPs) comprise sequence information to guide the cellular export of the encoded protein after translation. As IGF-I is a secreted protein, the potency of the mRNA and the subsequent expression and secretion of the translated IGF-I protein can be enhanced by engineering its SP.²⁵ In the present study, we engineered two IGF-I mRNA molecules with optimized SPs that potently improved the secretion compared with the endogenous IGF-I SP, enabling their use in local administration paradigms as outlined. Using these IGF-I mRNA molecules, we show that local injection of naked mRNA was therapeutically efficacious in regenerating skeletal muscle after injury and stopping degeneration after spinal disc herniation in animal models.

RESULTS

To demonstrate the regenerative potential of endogenous IGF-I mRNA (Cpd.1) in a severe muscle injury, we first demonstrate that the local intramuscular (i.m.) injection of IGF-I mRNA accelerated muscle regeneration. Subsequently, IGF-I mRNA was sequence engineered with heterologous SPs derived from human brain-derived neurotrophic factor (BDNF; Cpd.2) and neurotrophic factor 3 (NTF-3; Cpd.3) genes to improve the IGF-I protein secretion. *In vitro* and *in vivo* improvements of engineered IGF-I mRNA (Cpd.2) were assessed versus endogenous IGF-I mRNA (Cpd.1) in a mouse myotoxic injury. The pharmacokinetic (PK) and pharmacodynamic (PD) profile of Cpd.2 engineered IGF-I mRNA and its activation of IGF-I-mediated signaling pathway were verified *in vivo*. Finally, the regenerative potential of Cpd.3 engineered IGF-I mRNA was validated in rabbit spinal disc herniation model.

Cpd.1: Endogenous IGF-I *in vitro* transcription mRNA accelerates functional recovery in a mouse myotoxic injury model

To investigate the therapeutic benefit of tissue regeneration after injury by local treatment with *in vitro* transcription (IVT) mRNA encoding for human IGF-I guided by endogenous SP, a model of severe muscle injury was used. Injection of the snake venom notexin into the tibialis anterior (TA) muscle in adult mice induced a complete breakdown of muscle fibers and their neuromuscular connections that lasted for several days and morphologically and functionally recovered within a 3–4 week period.^{26–28} Because of the specific role of IGF-I in satellite cell biology and early myogenesis, this model appeared well suited to investigate IGF-I-mediated skeletal muscle repair mechanisms.

To define a baseline of muscle force in healthy animals, uninjured (sham) mice were assessed for TA muscle force and revealed an

average maximal force of 201 ± 28 mN ($n = 20$), ranging from 150 to 250 mN (Figure 1A), which defined the healthy range in Figure 1B. Injection of 0.4 μ g notexin into the TA muscle on day 0 resulted in immediate paralysis and a total loss of muscle force on days 1 and 4 in all treatment groups. On days 1 and 4, vehicle or Cpd.1 was injected each directly after force measurement. In the vehicle group, early signs of functional recovery were visible from day 7 on and reached the healthy range only by day 28 (Figure 1B), whereas treatment with 3 μ g Cpd.1 on days 1 and 4 resulted in a similar trajectory of slow functional recovery: the two doses of 10 and 30 μ g, applied on days 1 and 4 after injury, accelerated functional recovery immediately, visible by day 7 and resulting in full recovery by day 15 (Figure 1B). To assess the entire functional improvement from the treatment, an area-under-the-curve (AUC) analysis was performed over the entire time frame, which confirmed a 40%–50% improvement of muscle function after treatment with 10 and 30 μ g Cpd.1 (Figure 1C).

Subsequent to the functional testing, the structural and functional muscle composition was investigated, and TA muscles were collected on day 28 and histologically processed as described in Table S1 to count total fiber numbers, fiber size (cross-sectional area [CSA]) of individual fibers and relative contribution of MyHC type I, IIa, and IIb fibers. As controls, contralateral non-injured muscle fibers were identically processed and analyzed. Vehicle-treated animals with injury showed a significant increase in TA fiber count and a significant decrease in CSA, suggesting that injury has induced fiber hyperplasia and delayed myocyte maturation (i.e., more fibers that are smaller) (Figures 1D and 1E). Assessment of total fiber count after the study period revealed that in both vehicle and 3 μ g (but not 10 and 30 μ g) dose groups, significantly more total TA fibers were counted compared with the non-injured muscles, suggesting that successful treatment had prevented injury-induced fiber hyperplasia (Figure 1D). In agreement with this finding, both vehicle and 3 μ g (but not 10 and 30 μ g) dose groups had significantly smaller muscle fibers in the injured compared with non-injured muscles as assessed by CSA measurement, suggesting that successful treatment had prevented injury-induced fiber atrophy (Figure 1E). Finally, although the gross composition of slow type I vs. fast type IIa and IIb muscle fiber types had not significantly changed by injury and/or treatment (Figure 1F), in-depth investigation revealed a significant increase of slow muscle type I fibers in vehicle and 3 μ g groups compared with the 10 and 30 μ g dose groups in injured and compared with the contralateral non-injured muscle (Figure 1G). As slow type I fibers are the first fibers to develop following muscle injury and fast type II fibers occur later, these data suggest a delayed stage of structural regeneration in the injured muscles of the vehicle and 3 μ g groups on day 28, whereas in the 10 and 30 μ g groups regeneration has been accelerated toward full maturity by this time point.

In summary, the data confirm that i.m. application of IGF-I IVT-mRNA at a dose of 10 or 30 μ g significantly accelerated TA muscle regeneration in mice on functional and structural levels to reach full maturity 28 days after severe myotoxic injury.

Cpd.2: Engineered IGF-I mRNA boosts secretion of IGF-I protein *in vitro*

Encoding secretory proteins that act extracellularly through mRNA requires the cells to efficiently transfer the proteins into the exocytosis pathway. For this purpose, secretory proteins contain a SP sequence that is cleaved off within the cell before exocytosis.²⁵ In the case of IGF-I, the pre-pro-protein was encoded containing the SP in the 5' pre-domain, the 5' pro-domain and IGF-I functional domain. In Cpd.1, the natural sequence of human pre-pro-IGF-I was encoded, resulting in physiologically relevant protein expression and secretion of about 50 ng/mL into the supernatant 24 h after transfection of human embryonic kidney 293 (HEK293) cells (Figure 2A). We aimed to design an IGF-I mRNA with increased protein secretion through optimization of its SP and exchanged the natural SP by that of human BDNF (Cpd.2), another secretory growth factor.

Transfection of HEK293 cells with heterologous SP comprising IGF-I mRNA (Cpd.2) resulted in 3.3-fold higher IGF-I protein secretion into the supernatant after 24 h (Figure 2A). Analyzing the concentration dependence of Cpd.1 and Cpd.2 at 24 h after transfection, a 5- to 6-fold shift in potency (half maximal effective concentration [EC₅₀]) of Cpd.2 as observed compared with Cpd.1 was observed (Figure 2B). We further investigated the time dependence of Cpd.2 mRNA and protein translation within the cells after transfection and found that Cpd.2 mRNA resided in the cells with a half-life of ~17 h and led to protein expression and secretion with a peak within the first 24 h and physiologically relevant IGF-I levels over up to 3 days after transfection into HEK293 cells (Figure 2C). Further experiments in other cell types revealed a 6.1-fold increase of IGF-I secretion in a murine myoblast cell line (C2C12; Figure 2D) and a 3.1-fold increase of IGF-I secretion by human primary skeletal muscle cells (HskMCs; Figure 2E), suggesting a general potentiating effect through SP modification in cells relevant for the *in vivo* i.m. application. The IGF-I produced from Cpd.2 mRNA and secreted into the supernatants showed full bioactivity, as confirmed in a proliferation assay using MCF-7 breast cancer cells. When seeded at 3,000 cells/well, a concentration-dependent increase in ATP with an EC₅₀ of 3 ng/mL was observed for both Cpd.2 and INCRELEX, a human recombinant IGF-I that has been approved for clinical use (Figure 2F). IGF-I efficacy was confirmed also at a higher cell density of 10,000 cells/well (Figure S1), showing comparable bioactivity of mRNA-derived and clinically used IGF-I. No statistical difference between the Cpd.2 and INCRELEX groups was observed (Figures 2F and S1).

On the basis of these data, by optimization of the SP, decent potentiation of functional IGF-I was achieved, and both the increase in total IGF-I secretion (2- to 6-fold) and enhanced potency (~6-fold) of Cpd.2 predicted a major improvement of *in vivo* potency compared with Cpd.1.

Cpd.2: Engineered IVT IGF-I mRNA demonstrates improved *in vivo* potency compared with endogenous IGF-I mRNA in the mouse model of myotoxic injury

In this study, the analysis of TA muscle force of healthy, uninjured (sham) mice yielded an average maximal force of 247 ± 33 mN

(n = 30), ranging from 190 to 290 mN (Figure 3A); the healthy range is defined in Figure 3B. Injection of 0.4 µg notexin into the TA muscle on day 0 fully reproduced previous findings, with immediate paralysis, a total loss of muscle force measured on days 1 and 4 after vehicle injection, and functional recovery starting on day 7 and reaching near healthy levels by day 28 (Figure 3B). Direct comparison of a 10 µg dose of Cpd.1 with a 1 µg dose of Cpd.2 showed very similar acceleration of functional recovery in this model (Figure 3B). The AUC analysis confirmed the nearly identical improvement of muscle function over the 28 day period after treatment with 10 µg Cpd.1 or 1 µg Cpd.2 (Figure 3C). To characterize the *in vivo* potency improvement for Cpd.2 with heterologous SP in the myotoxic injury model more precisely in comparison with Cpd.1, the full dose response of Cpd.2 (0.05–30 µg) was compared with Cpd.1 (3–30 µg). EC₅₀ values were 0.4 µg for Cpd.2 and 6.6 µg for Cpd.1, suggesting a 15-fold improvement of *in vivo* potency for Cpd.2 over Cpd.1 (Figure 3D). At doses of 3 µg or higher, a bell-shaped effect curve was observed for Cpd.2, suggesting a biological desensitization effect upon overdosing. In contrast, local concentrations of IGF-I after Cpd.1 injection did not reach levels needed to desensitize the IGF receptors.

In summary, the comparative study in the myotoxic injury model confirmed a 15-fold increase in the potency of the IGF-I mRNA by using an optimized SP to enhance cellular secretion. Furthermore, the bell-shaped form of the dose-response curve strongly indicated a physiological activation of the IGF-IR pathway by mRNA-induced local IGF-I delivery and subsequent receptor desensitization at higher concentrations.

PK and PD profile of Cpd.2: Engineered IVT IGF-I mRNA in a rat muscle punch injury model

To exert relevant biological effects of mRNA-based protein therapies, we investigated time and spatial distribution of Cpd.2 within the tissue and correlated it to protein production and biological downstream processes resulting in functional changes in a physiological manner. Therefore, mRNA distribution, IGF-I expression and downstream biological effects of i.m. Cpd.2 injection were assessed in an injury-dependent context. A severe, localized punch injury in the TA muscle of adult rats was applied, and Cpd.2 was injected directly thereafter at different doses (1, 3, or 10 µg) left and right of the injury. At different times after injury and treatment (6, 24, 48, and 72 h), muscles were dissected and tissue pieces of 4 mm thickness, each were collected at increasing distance from the injection site, with left (1L, 2L, 3L, 4L) pieces processed for RNA analysis and right (1R, 2R, 3R, 4R) pieces for protein analysis according to the scheme illustrated in Figure 4A.

After i.m. injection into the TA muscle, Cpd.2 showed dose- and time-dependent distribution exemplified for the 1L segment over up to 72 h (Figure 4B). Total exposure from 0 to 72 h was assessed using qPCR from extracted mRNA in an AUC analysis and revealed for both 1L and 2L dose-dependent Cpd.2 exposure with lower levels in 2L and undetectable Cpd.2 levels in 3L and 4L, similar to vehicle-treated muscles (Figure 4C). This suggests a limited spatial

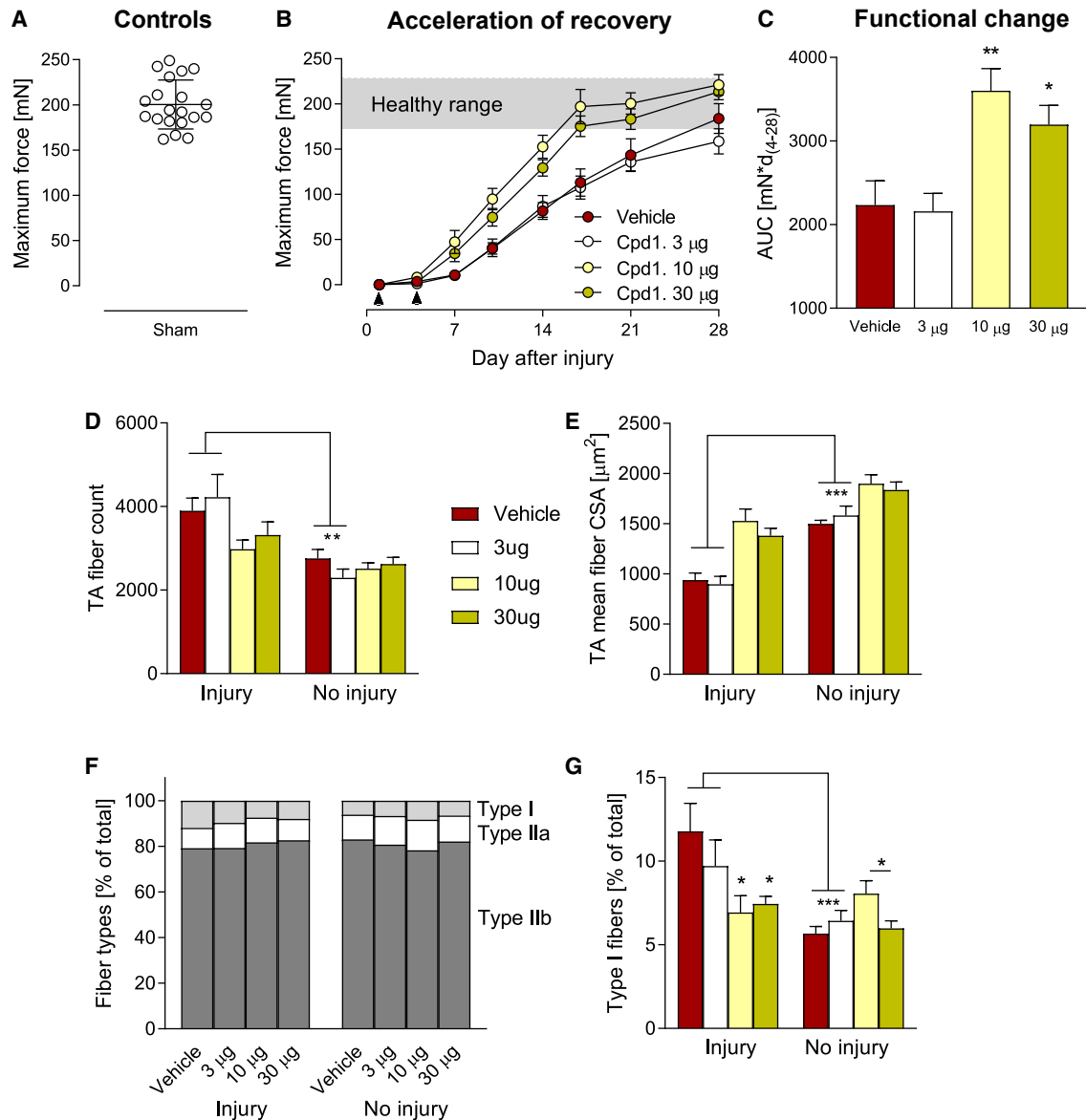


Figure 1. Acceleration of functional muscle regeneration by endogenous IGF-I mRNA (Cpd.1) in a mouse model of myotoxic injury

(A) Baseline of TA muscle force in healthy mice. (B) Functional recovery of paralyzed TA muscle with vehicle or increasing dose of Cpd.1 mRNA treatment measured by muscle performance over the course of 28 days. (C) Area-under-the-curve (AUC) analysis of muscle performance data (* $p < 0.05$, 30 µg versus vehicle; ** $p < 0.01$, 10 µg versus vehicle). (D) Histological measurement of total TA muscle fiber count in legs of injured and contralateral (uninjured) animals treated with vehicle or increasing dose of Cpd.1 (** $p < 0.01$, vehicle and 3 µg in injured versus uninjured). (E) Mean fiber cross-sectional area (CSA) in legs of injured and contralateral (uninjured) animals treated with vehicle or increasing dose of Cpd.1 (** $p < 0.001$, vehicle and 3 µg in injured versus uninjured). (F) Frequency of TA muscle fiber types measured by antibodies against MyHC-I, MyHC-IIa, and MyHC-IIb in legs of injured and contralateral (uninjured) animals treated with vehicle or increasing dose of Cpd.1. (G) Frequency of slow muscle type I fibers in legs of injured and contralateral (uninjured) animals treated with vehicle or increasing dose of Cpd.1 (** $p < 0.001$, vehicle and 3 µg in injured versus uninjured; * $p < 0.05$, 10 and 30 µg in injured versus uninjured; * $p < 0.05$, 10 and 30 µg uninjured). Data represent mean \pm SEM of 7–10 mice per group.

distribution of mRNA within the TA muscle after i.m. injection. Reliable half-life estimations for Cpd.2 were possible for the 3 and 10 µg doses in 1L and the 1 µg dose in 2L and yielded time-dependent and consistent exposure with a half-life of 17–25 h (Figure 4D). This mRNA residence within the muscle for up to three days resulted in

expression and secretion of human IGF-I in 1R of up to 18 pg/mg protein, well in the therapeutically relevant range. Thereby, time profiles of IGF-I exposure were more prolonged at the higher doses (Figure 4E), suggesting a distribution of IGF-I protein within the tissue according to indirect PD response model.²⁹

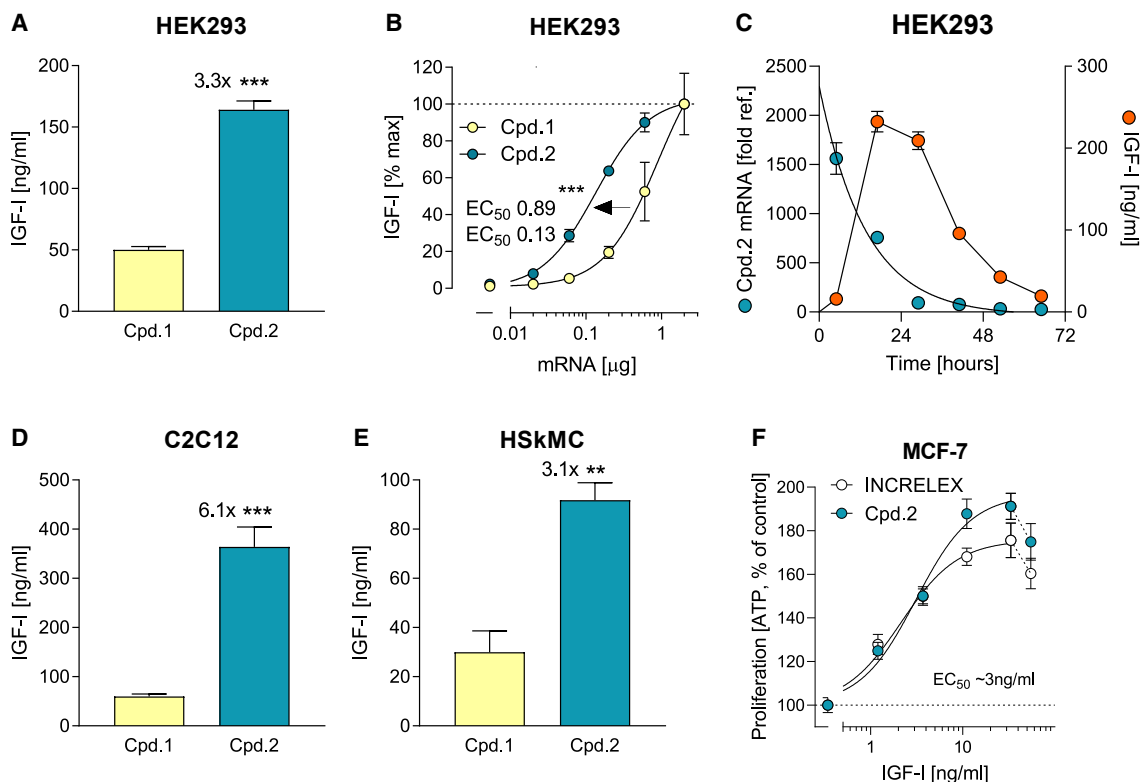


Figure 2. Improvement of IGF-I secretion through signal peptide optimization

(A) HEK293 cells were transfected Cpd.1 and Cpd.2 IGF-I mRNA using lipofection, and IGF-I protein was analyzed in the supernatant after 24 h using ELISA. Statistical analysis was carried out using Student's t test (** $p < 0.001$). (B) Dose-response study on induction of IGF-I secretion in HEK293T cells after mRNA transfection with Cpd.1 or Cpd.2. Cells were transfected with Cpd.1 or Cpd.2 at different concentrations (0, 0.02, 0.06, 0.2, 0.6, or 2 μg), and secreted IGF-I was measured after 24 h in the cell culture supernatant using a specific ELISA. Cpd.2 induced IGF-I secretion significantly more potent ($\text{EC}_{50} = 0.13 \mu\text{g}$) than Cpd.1 ($\text{EC}_{50} = 0.89 \mu\text{g}$). Data represent mean \pm SEM of 2 replicates. Significance (** $p < 0.001$) was assessed using two-way ANOVA of the two curves. (C) Time course study of Cpd.2 IGF-I mRNA and IGF-I protein levels in HEK293 cells. The time points at which RNA and IGF-I quantified include 5, 17, 29, 41, 53, and 65 h. The mRNA levels are measured by relative gene expression method ($2^{-\Delta\Delta\text{Ct}}$) where untransfected samples were used as control group and the expression level set to 1. Expression was normalized using human PPIA as a reference gene. Secreted IGF-I was measured in the cell culture supernatant using ELISA with respective time point. (D) IGF-I secretion from mouse skeletal muscle cells (C2C12) by mRNA transfection with Cpd.1-Cpd.2. C2C12 cells were transfected with each 2 μg Cpd.1-Cpd.2, and secreted IGF-I was measured after 24 h in the cell culture supernatant using a specific ELISA. Cpd.2 induced IGF-I secretion significantly higher than Cpd.1 (6.1-fold). Data represent mean \pm SEM of 4 replicates. Significance (** $p < 0.001$) was assessed using Student's t test. (E) Induction of IGF-I secretion from human primary skeletal muscle cells (HSkMCs) by mRNA transfection with Cpd.1 and Cpd.2. HSkMCs were transfected with each 2 μg Cpd.1 or Cpd.2, and secreted IGF-I was measured after 24 h in the cell culture supernatant using a specific ELISA. Cpd.2 induced IGF-I secretion significantly higher than Cpd.1 (3.1-fold). Data represent mean \pm SEM of 3 replicates. Significance (** $p < 0.01$) was assessed using Student's t test. (F) Proliferation assay with MCF-7 cells with increasing concentration of rhIGF-I (INCRELEX) or IGF-I derived from HEK293 cells supernatant transfected with Cpd.2 mRNA. Dose-response curve of MCF-7 cells (3,000 cells/well) after 96 h with treatments was plotted with four parameter non-linear fitted curve. No statistical difference between Cpd.2 and INCRELEX group was observed.

In 2R, low levels of IGF-I were measured near the detection limit of the assay, assuming less IGF-I production (Figure S2A). The IGF-I levels especially seen in 1R but partly also 2R segments were considered well in the range of physiological concentrations required for downstream signal activation. We therefore assessed AKT phosphorylation in the 1R and 2R samples. Because of the wound closure process an initial decline of AKT signaling was observed over 24 h in 1R, and only thereafter a dose-dependent increase of AKT phosphorylation by Cpd.2 treatment was observed (Figures S2B and S2C). In contrast, in 2R (without the injury) reliable AKT phosphorylation revealed a dose-dependent and prolonged increase in phosphorylated AKT (pAKT)/AKT ratio (Fig-

ure 4F). Analyzing the correlation between IGF-I expression in 1R and AKT phosphorylation in 2R revealed good correlations for the 1 and 3 μg doses and a fair correlation for the 10 μg dose (Figures S2D–S2F), suggesting that locally expressed and secreted IGF-I induced downstream signaling within the TA muscle with a spread of 4–8 mm from the injection site.

In summary, the data confirmed that after a single injection into the rat TA muscle in context of an injury, Cpd.2 exposure was sustained over 3 days with a half-life or ~ 20 h, resulted in time-dependent local IGF-I production over that time frame that induced downstream signaling of the IGF-IR pathway.

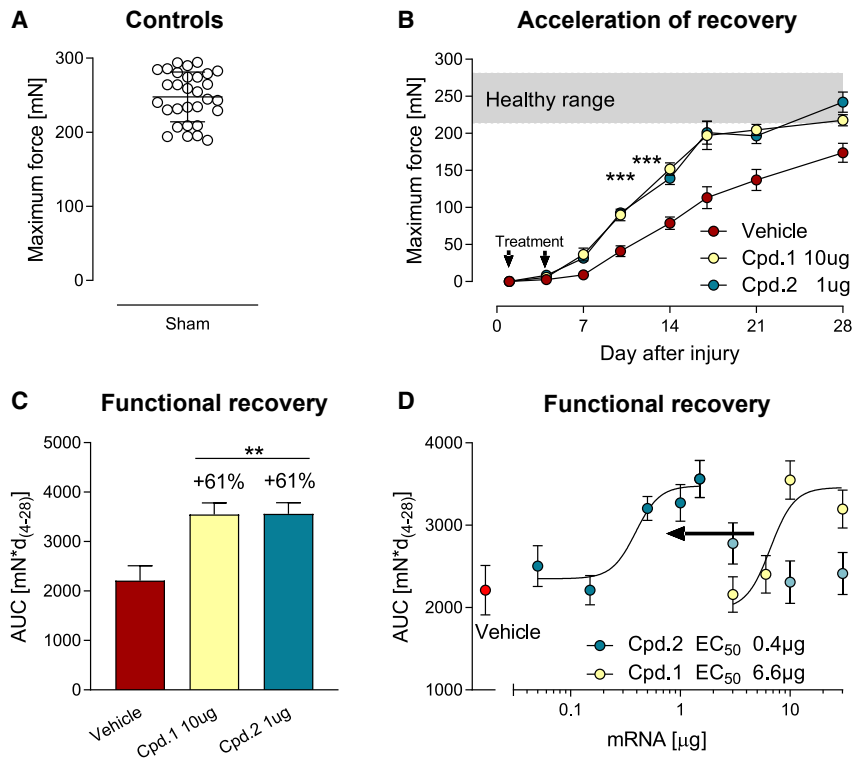


Figure 3. Comparison of endogenous and optimized IVT IGF-I mRNA in mouse myotoxic injury model

(A) Muscle function of non-injured TA muscles. TA muscles from non-injured animals ($n = 10$) were assessed for muscle function on days 7, 14, and 28 each, and data were sampled. Data are from a total of $n = 30$ measurements. (B) Functional recovery of TA muscle after notexin injury. After notexin injury via intramuscular injection (day 0), IGF-I mRNA treatments (Cpd.1, 10 μ g; Cpd.2, 1 μ g) were applied by intramuscular injection on days 1 and 4 (see arrowheads). The control group received vehicle solution. Muscle function was assessed on days 1, 4, 7, 10, 14, 21, and 28 post-injury. Data represent mean \pm SEM of 5 mice per group and time point. A 2-way ANOVA revealed highly significant difference between both Cpd.1 and Cpd.2 curves compared with vehicle ($***p < 0.001$). (C) Area-under-the-curve (AUC) calculation of functional recovery after myotoxic injury. Animals were subjected to notexin injury on day 0, and Cpd.1 or Cpd.2 at indicated doses or vehicle was injected i.m. on days 1 and 4. TA muscle function was assessed on days 4, 7, 10, 14, 17, 21, and 28 from the same mice, and AUC was calculated from each animal. Data are represented as mean \pm SEM, with 4 or 5 animals per group. Statistical analysis was done using a one-way ANOVA followed by Dunnett's multiple-comparison test. $**p < 0.01$ vs. vehicle. (D) Dose-response curves (0.05–30 μ g) from AUC of functional recovery after myotoxic injury. Animals were subjected to notexin injury on day 0, and Cpd.2 or Cpd.1 at indicated

doses or vehicle injected i.m. on days 1 and 4. TA muscle function was assessed on days 4, 7, 10, 14, 17, 21, and 28 from the same mice, and AUC for maximum force was calculated from each animal. From the XY plots, EC₅₀ values were calculated to 0.4 μ g for Cpd.2 and 6.6 μ g for VMB-Cpd.1 by a non-linear Hill fit. Data are represented as mean \pm SEM, with 4–14 animals per group.

Regulation of key downstream biomarkers by Cpd.2: Engineered IVT IGF-I mRNA in a rat muscle punch injury model

Having shown that exposure and IGF-IR activation can be induced by a single application of IGF-I into the injured rat TA muscle, we further analyzed key processes of early muscle regeneration after skeletal muscle injury in the 1L and 2L segments over 72 h after injury. The scheme in Figure 5A (adapted from Ciciliot and Schiaffino³⁰) illustrates the time course of molecular and cellular processes during early regeneration after skeletal muscle injury, and the relevance of key proteins for specific processes. Further illustration of relevant biomarkers for myogenic repair which were analyzed in this study is shown in Figures S3A and S3B. On the basis of the hypothesis that severe injuries such as the applied punch injury induces rapid reactivation of satellite cells, we analyzed endogenous Pax7 mRNA and observed a slight upregulation after 72 h in 1L but not 2L in vehicle-treated muscles (Figure 5B). Treatment with 3 μ g Cpd.2 induced a strong potentiation and acceleration of the Pax7 upregulation already after 24 h in 1L and 48 h in 2L, whereas 1 and 10 μ g Cpd.2 doses induced only a minor change of Pax7, similar to the endogenous response (Figure 5B). Expression of MYH3, the embryonic form of myosin occurring later in the process once new muscle fibers have been generated, was endogenously upregulated after 72 h, an effect that was strongly potentiated by 3 μ g Cpd.2, with a stronger response in 2L compared with 1L (Figure 5C). Both Pax7 and MYH3 effects suggested that the biological effects through Cpd.2 treatment extended beyond the injury into 2L. Analysis

of further key biomarkers MyoD1, Myf5, or MyoG showed similar time- and space-dependent induction with the 3 μ g Cpd.2 dose (Figures S4A–S4C). In contrast, MYH8 and MYH4, myosin variants expressed by later developing more mature muscle fibers, did not show a change either by the injury or by Cpd.2 treatment within 72 h (Figures 5D and S4D).

In summary, the investigation of a 72 h time frame after a severe punch injury in rat TA muscle provided evidence that the IGF-I produced by Cpd.2 could potentiate the endogenous myogenic repair processes. Thereby, the bell-shaped dose relation observed in the myotoxic injury model was confirmed in the punch injury model with optimal doses at exactly the same Cpd.2 levels (3 μ g Cpd.2) and indication for desensitization at the higher dose 10 μ g Cpd.2, highlighting the appropriate dosing regimen necessary to achieve biological responses.

Cpd.3: Engineered IVT IGF-I mRNA delays pathology progression in a rabbit model of spinal disc herniation

To confirm the general regenerative capacity of IGF-I mRNA beyond skeletal muscle injuries and to provide insights in its efficacy in a more delayed treatment setting, we investigated the benefit of another SP-optimized form of IGF-I mRNA (Cpd.3) in a delayed setting of spinal disc injury in adult rabbits. The therapeutic rationale for IGF-I benefit in spinal disc herniation has been confirmed in multiple studies

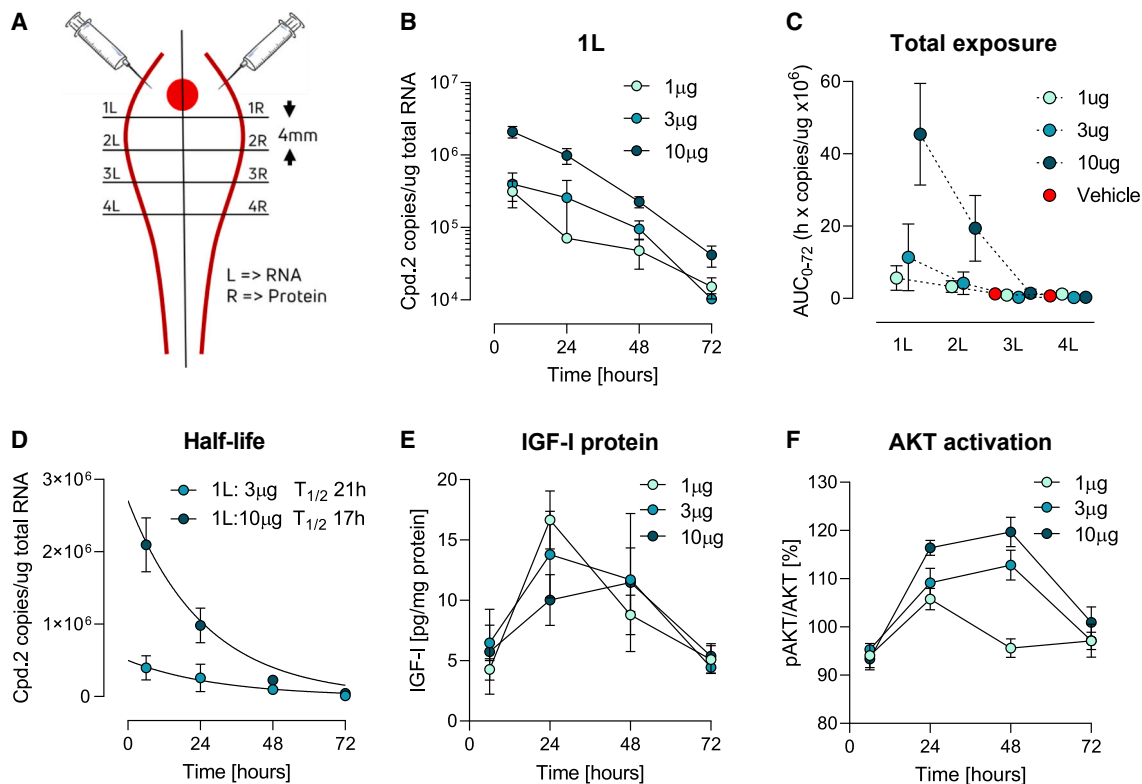


Figure 4. PK/PD of IGF-I mRNA in rat TA muscle

(A) Scheme of TA muscle processing and generation of tissue pieces. The red circle indicates the site of the punch injury and 1L and 1R where Cpd.2 injections had been located. Segments 1L–4L were processed for qPCR analysis of Cpd.2 and downstream biomarkers, segments 1R–4R were processed for protein analysis of IGF-I and pAKT. (B) Time course of Cpd.2 mRNA exposure in TA muscle of 1L segment at time points 0–72 h after i.m. injection by qRT-PCR. (C) AUC analysis (0–72 h) to measure mRNA exposure from 1L to 4L at different doses (1, 3, or 10 µg) and vehicle treatment. (D) Half-life of Cpd.2 exposure in 1L and 2L segment, assessed for the 3 and 10 µg doses. (E) IGF-I protein expression after i.m. injection of 3 or 10 µg Cpd.2, at time points 0–72 h. 1R muscle samples were taken and analyzed for IGF-I protein by iQELISA. (F) Tissue phosphorylation of AKT as downstream signal of IGF-I at time points 0–72 h after i.m. injection of Cpd.2 in TA muscle. 2R muscle samples were taken and analyzed for phosphorylation of AKT at Ser473 by a phosphor-specific and total AKT ELISA kit. Data are expressed as area under the curve (AUC) and represent mean ± SEM of 8 animals per group.

in vitro, *in vivo*, and by epidemiological evidence.^{8,31–33} Cpd.3 contained the SP sequence (pre-domain) of NTF-3, another secretory growth factor, and otherwise the natural IGF-I pro-domain and coding region. We selected Cpd.3 for a rabbit model of spinal disc herniation instead of Cpd.2 on the basis of the expression advantage we noticed in primary motoneurons and IMR32 neuroblastoma cells (Figure S5). *In vitro* transfection with 300 ng Cpd.3 demonstrated a robust induction in IGF-I protein secretion in HEK293 cells, HepG2 cells, and rat motoneurons that outperformed Cpd.1 (with the natural SP) by 2.3-fold (Figure 6A), 3.5-fold (Figure 6B), and 4.6-fold (Figure 6C), respectively. The data confirmed a general IGF-I secretion-potentiating effect in different cell types by exchange of the SP in Cpd.3.

For the spinal disc herniation rabbit model, the injury was placed into the L2/L3 and L4/L5 intersections on day 0 using a stab. Thereafter, animals were allowed to recover and to develop the spinal degeneration for 30 days followed by four weekly treatments through local in-

traspinal injection of 20 µg Cpd.3 until day 51 after injury. Thereafter, animals were further observed until day 90 with regular X-ray and body weight assessments. Figure 6D outlines the group allocation scheme which has been performed in a total of 8 adult rabbits, each serving as its own control by receiving vehicle solution into the L2/L3 disc (vehicle), a sham procedure without injury in the L3/L4 disc (sham), and 20 µg Cpd.3 into the L4/L5 disc (Cpd.3). Figure 6E illustrates the optical control of the puncture injury process using a stab, and Figure 6F shows the X-ray analysis of the intersections and discs before and after injury/treatment. Over the entire 90 days period, all animals gained weight, and none of them demonstrated any general negative impact of the procedure (Figure 6G). Analysis of the disc height index (DHI) on days 0 (before injury), 30 (at treatment start), 60, and 90 (after injury) showed that the sham-treated discs (L3/L4) appeared stable, without any signal of deterioration (Figure 6H). In contrast, vehicle-treated injured discs (L2/L3) of the same rabbits showed a progressive decline in disc space assessed and reported as DHI (Figure 6H). Treatment with Cpd.3 for 4 weeks

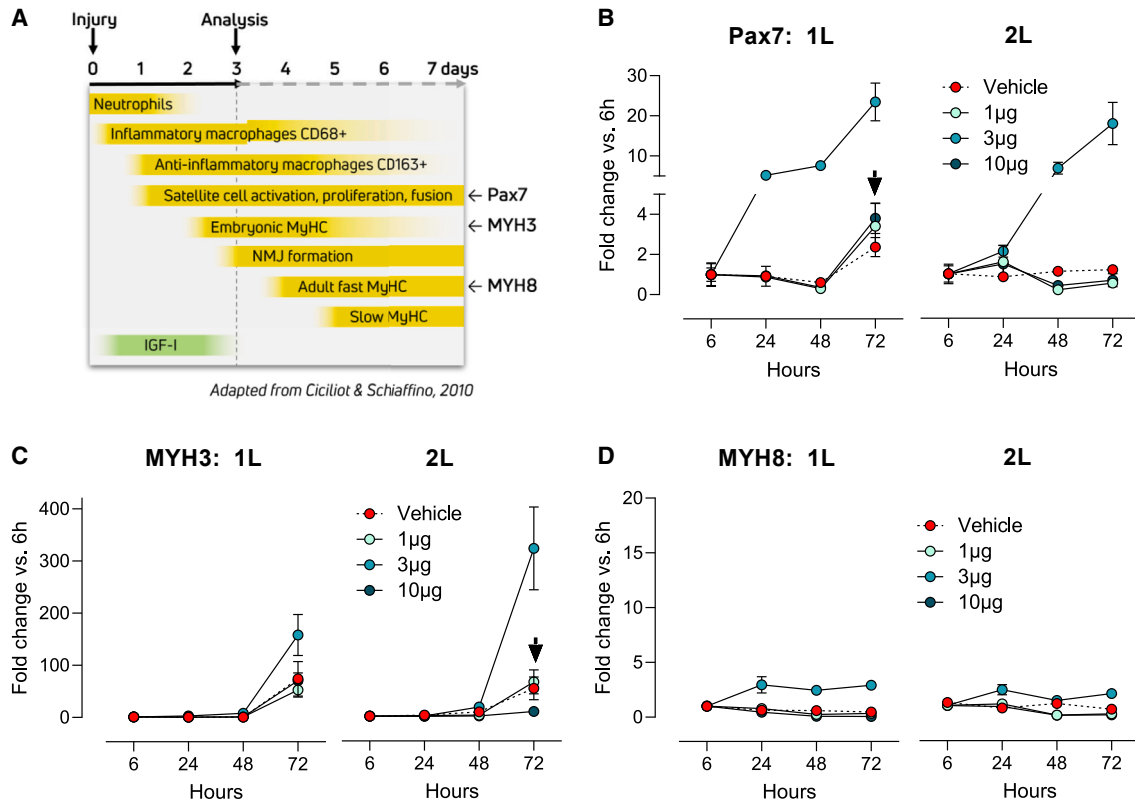


Figure 5. Changes in downstream biomarkers expression in rat injury model

(A) Illustration of skeletal muscle regenerative process within 7 days after injury. Early processes within the first three days include processes of inflammation and satellite cell activation, proliferation, and fusion, but also early myogenic processes including embryonic myosin isoforms to be expressed, whereas adult myosins are only expressed after that time period. Pax7, MYH3, and MYH8 were investigated for their time course over three days after injury and the potential change due to Cpd.2 treatment (adapted from Ciciliot and Schiaffino³⁰). (B–D) qPCR analysis of Pax7, MYH3, and MYH8 mRNA levels after muscle injury. Punch injuries were applied to TA muscle in rats, and vehicle or Cpd.2 applied i.m. at different doses (1, 3, or 10 µg) directly after injury as described. At times indicated, tissues were harvested and analyzed for Pax7, MYH3, and MYH8 using qRT-PCR. Relative changes were calculated by normalizing individual values to the respective control of each treatment group. Dose dependence and time course of these 3 markers were investigated in 1L and 2L segment. Arrows point to changes occurring 3 days after injury. Data are expressed as mean ± SEM of 5 (vehicle) and 8 (Cpd.2 dose groups) animals per data point. Gray dashed line indicates the control level of 1.

starting on day 30 resulted in a subsequent stop in progression of the degenerative process and a highly significant improvement of DHI after 90 days compared with the vehicle group (83% vs. 72%; Figure 6H).

After 90 days, all animals were sacrificed, and spines and discs processed for histology by toluidine blue and Masson's trichrome staining (Figure 7A). A semiquantitative analysis was performed investigating the status and preservation of the annulus fibrosus (AF), its border to the nucleus pulposus (NP), and the cellularity and matrix of the NP quantified by each of three categories outlined in Table S3, and revealing a significant deterioration of tissue integrity in the vehicle-treated discs and a >60% improvement in Cpd.3-treated discs compared with the sham-treated uninjured discs (Figures S6A and S6B). A composite histology score was derived from these individual analyses showing a highly significant deterioration in parameters in vehicle-treated discs compared with the sham-treated discs (Figure 7B). Treatment with Cpd.3 led to an improve-

ment of the composite score toward healthy levels, not significantly different from sham-treated discs (Figure 7B).

In summary, the data generated in the spinal disc model with SP-optimized IGF-I mRNA (Cpd.3) demonstrated that the regenerative and preventive effect of IGF-I administered via local mRNA injection into the damaged environment is capable to stop the progression of deterioration even in a delayed, non-acute setting with fully established pathology.

DISCUSSION

The recent success of mRNA-based pharmaceuticals in developing the COVID-19 vaccines with speed created unprecedented credibility for this technology. Beyond vaccines, mRNA-based medicine has tremendous potential for protein replacement therapy as the modality provides key advantages over recombinant proteins and gene therapy, including physiological expression levels, tunable kinetics, an improved safety profile, and the prospect of repeated

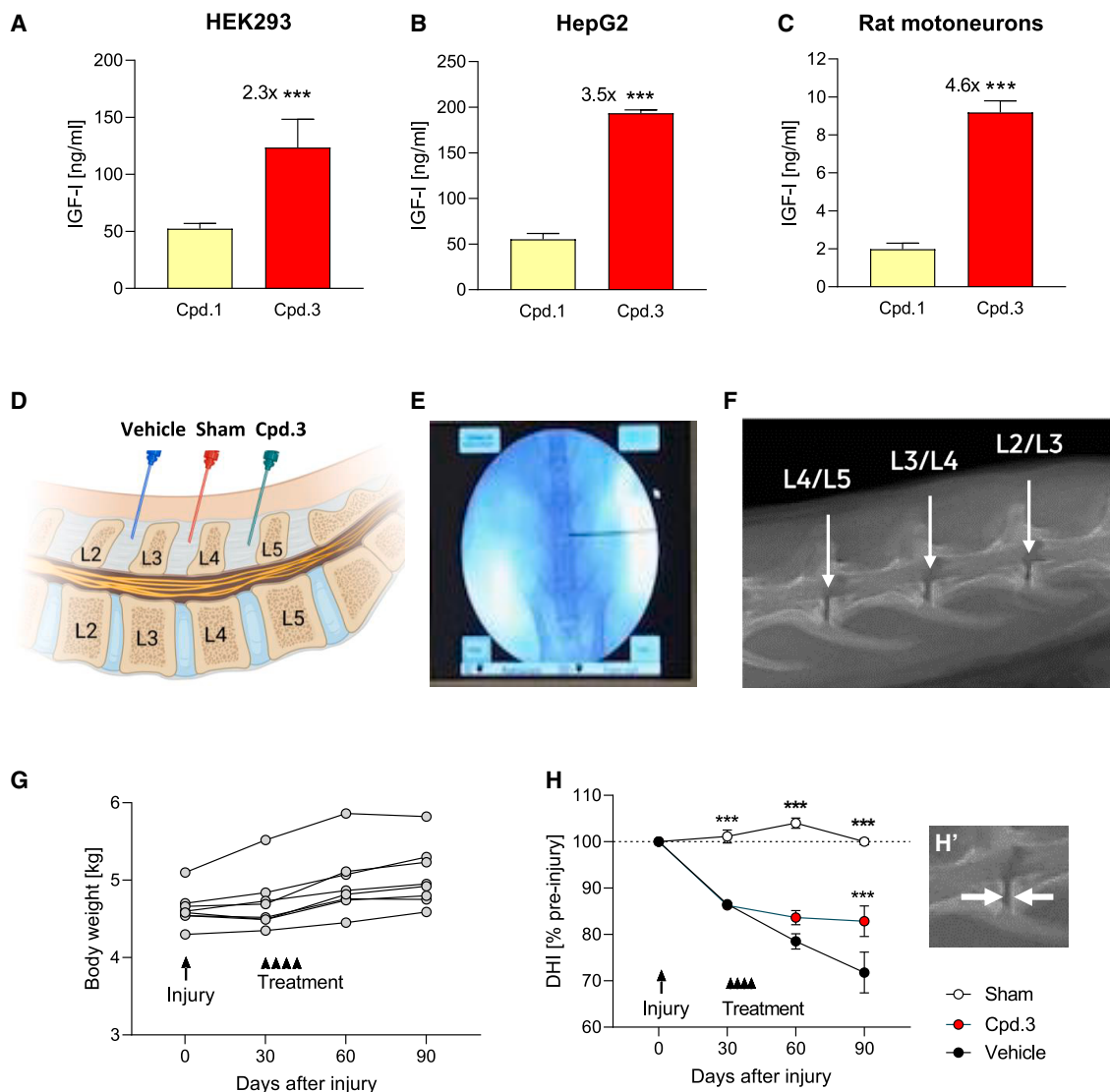


Figure 6. Prevention of functional deterioration in rabbit spinal disc herniation model

(A) *In vitro* assessment of Cpd.1 and Cpd.3 mRNA (300 ng/well) based expression and secretion of IGF-I in HEK293 cells (12,000 cells/well). (B) *In vitro* assessment of Cpd.1 and Cpd.3 mRNA (300 ng/well) based expression and secretion of IGF-I in HepG2 cells (20,000 cells/well). (C) *In vitro* assessment of Cpd.1 and Cpd.3 mRNA (300 ng/well) based expression and secretion of IGF-I in primary rat motoneurons (10,000 cells/well). All three cell types were transfected with Cpd.1 and Cpd.3 IGF-I mRNA using Lipofectamine 2000, and IGF-I protein was analyzed in the supernatant after 24 h using ELISA. Statistical analysis was carried out using a Student's t test (***p* < 0.001). (D) Schematic presentation of group allocation for treatments and each rabbit (*n* = 8) serving as its own control by receiving vehicle solution into the L2/L3 intervertebral space (vehicle), a sham procedure without injury in the L3/L4 disc (sham), and 20 μg Cpd.3 into the L4/L5 intervertebral space (Cpd.3). (E) Optical control of the puncture injury process using a stab. (F) X-ray picture to indicate L2/L3, L3/L4, and L4/L5 discs. (G) Body weight evolution of animals during the study over period of 90 days. Each line corresponds to one animal, and all eight-animal data are included with the measurement day. (H) Changes in the intervertebral disc height index (%DHI) in function of treatment. (H') Calculation of disc height. Data are expressed as mean ± SEM of 8 rabbits. Statistical comparison was done using 2-way ANOVA and Dunnett's multiple-comparison test against saline group.

dosing.^{34,35} Moreover, new evidence from vascular endothelial growth factor A (VEGFA) mRNA, AZD8601, to stimulate regenerative angiogenesis in patients with type 2 diabetes mellitus and cardiovascular disease provides proof of concept for the implementation of mRNA-based drug modalities in regenerative medicine.^{36,37} The role of IGF-I has been well established as a key factor in muscle repair and tissue regeneration. However,

the clinical translation of recombinant IGF-I was hampered by an undesirable PK profile, resulting in safety issues associated with the short exposure period and ineffective delivery methods.³⁸ The respective challenges could be resolved by more homeostatic kinetics of IGF-I delivery and the feasibility of local administration to prevent systemic side effects, both offered by mRNA-based therapeutics.³⁶

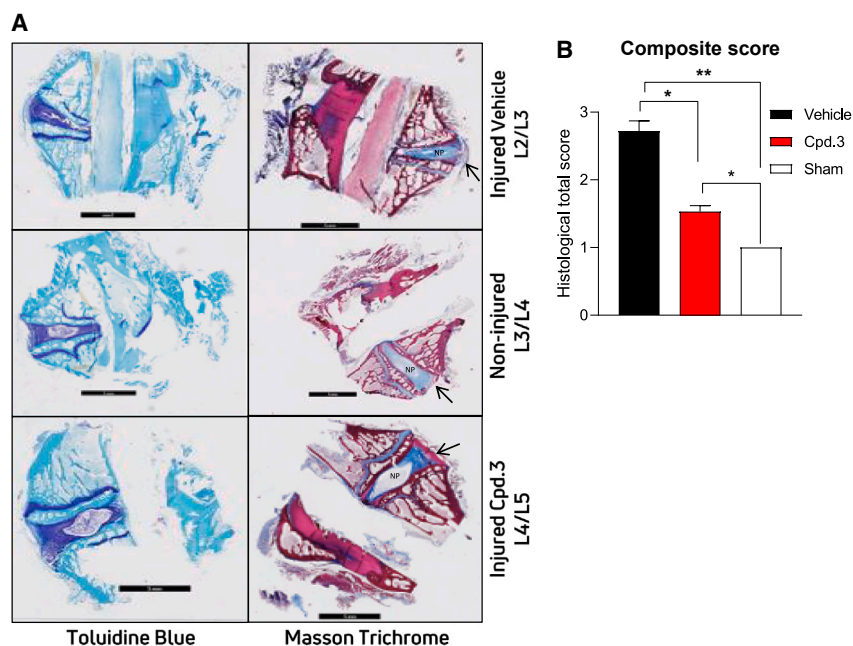


Figure 7. Prevention of pathological progression in rabbit spinal disc herniation model

(A) Representative histological pictures of the vehicle-treated, sham-treated, and Cpd.3-treated discs stained with toluidine blue and Masson's trichrome. (B) Histological grading score derived from vehicle-treated, sham-treated, and Cpd.3-treated discs. Data are expressed as mean \pm 95% CI of 8 rabbits. Statistical comparison was performed using the non-parametric Mann-Whitney test between all groups.

pAkt activation over 1–2 days, resulting in physiological stimulation of muscle regeneration.^{17,36,37,40}

Biomarker analyses confirmed the ability of Cpd.2 to activate satellite cells and to stimulate the development of new muscle fibers as measured by Pax7 and MYH5 over expression, respectively.^{3,5,41} However, we observed that high-dose Cpd.2 mRNA (10 μ g) resulted in negative impact on biomarkers expression and IGF-I protein expression. We presume the observed effect is due to the combination of factors including bell-shaped effect induced by IGF-IR desensitization due to excessive IGF-I levels,^{42–45} and the inherent dynamics of endogenous biological processes, including translation.^{46,47}

Additionally, IGF-I signaling is expected to be negatively cooperated, similar to insulin, which may provide further evidence, that high IGF-I concentrations may induce autoinhibition leading to bell-shaped dose-response curves.⁴⁸

The local injection of NTF-3 SP engineered IGF-I mRNA in a rabbit model of spinal disc herniation showed the capacity of the test compound to stop disease progression and disc height loss. Gene expression analyses in a similar rabbit model confirmed the link between IGF-I deficiency and disc degeneration.³³ Moreover, a genetic epidemiological study reported an association of IGF-I signaling with spinal disc degeneration in postmenopausal women,⁴⁹ which supports the value of IGF-I mRNA therapy as viable treatment option. Overall, the assumption of improving IGF-I mRNA potency by using heterologous SP was successful and paved the way to resolve the volume-related dose limitation and drug-related side effects.^{24,50} Both engineered IGF-I mRNAs exhibited a pre-clinically meaningful benefit for accelerated healing and prevention of functional deterioration.

The COVID-19 vaccine mRNA (BNT162b2) formulated in LNPs has been observed to leak from the injection site into the blood and was detected in the circulation after several days post-vaccination.⁵¹ Because of increased potency, our engineered IGF-I mRNA was applied at 10–30 times lower concentrations, and consequently no systemic exposure was found at any time point in tested animal models (data not shown). As we opted to induce regeneration locally at the site of injury, the engineered IGF-I mRNA was administered in a naked form using a simple citrate-buffered saline

Here, we investigated the regenerative power of IVT IGF-I mRNA in animal models of severe muscle injury and spinal disc herniation. Our data on muscle injury demonstrated that the local i.m. injection of endogenous IGF-I mRNA accelerated muscle regeneration and reduced fiber atrophy and hyperplasia. Moreover, optimization on mRNA level resulted in an increased potency. Earlier investigations have shown that SPs are critical for protein secretion, and replacement of SP with those from proteins known for higher secretion is an attractive option to improve the protein expression.³⁹ In this study, we engineered the IGF-I mRNA with heterologous SP from BDNF and NTF-3 to enhance IGF-I secretion. Our results showed that engineered IGF-I mRNA was translated into 6-fold increased levels of IGF-I protein compared with the endogenous counterpart at the same concentration *in vitro*, IGF-I potency in functional model systems was further shifted by a similar factor, suggesting that SP engineering plays an essential role, especially at low mRNA concentrations. The enhancement of EC₅₀ of IGF-I with Cpd.2 comprising BDNF SP is potentially due to the optimal amino acid sequence composition that boosted endoplasmic reticulum (ER) translocation efficiency and superior folding capacity over endogenous IGF-I SP.²⁵ Head-to-head comparison of native IGF-I mRNA and BDNF-SP engineered IGF-I mRNA (Cpd.2) for functional recovery in a mouse myotoxic injury model revealed that the engineered molecule is 16-fold more efficacious than non-engineered IGF-I mRNA, confirming this hypothesis. The number of mRNA molecules taken up by each cell *in vivo* is expected to be lower than in an *in vitro* cell culture setting, in which artificial transfectants such as Lipofectamine 2000 are being used and protein translation might be saturated because of a smaller number of cells and transfection related cell death.

The PK/PD analysis of Cpd.2 in a rat muscle punch injury model revealed homeostatic, extended kinetics for both IGF-I expression and

solution into muscle or disc. Intradermal injection of VEGFA mRNA (AZD8601) formulated in citrate-buffered saline induced efficacious VEGFA levels in patients with type 2 diabetes mellitus.³⁷ Likewise, direct epicardial injections of VEGFA mRNA after an elective coronary artery bypass surgery was found to be very safe and to improve the left ventricular ejection fraction.³⁶ Moreover, it was reported that in cardiac muscle, the direct injection of naked mRNA formulated with simple buffers (sucrose citrate or saline) revealed a superior protein expression (>50- to 200-fold) compared with LNPs or polymers, possibly because of the translational hindrance of nanoparticles in muscle matrix.²² Interestingly, Hotz et al.⁵² reported that a direct intratumoral administration of four cytokines encoding mRNA (IL-12, IFN- α , GM-CSF, and IL-15 sushi) formulated in saline established an effective and strong antitumor activity. Several other investigations supported the use of naked mRNA in lungs, skin, lymph nodes, vagina, and muscles.^{53–55} The exact mechanism of how naked mRNA macromolecule diffuses across the cellular membrane despite negative charges remains unclear. However, uptake by scavenger receptors, hydrodynamic pressure, macropinocytosis, and the endocytotic pathway are proposed as a cellular process that aids naked mRNA for cellular internalization.⁵⁶ In this study, we did not explore the mechanism of uptake but rather focused on therapy development. Similarly, we observed expression of functional IGF-I levels leading to induction of downstream signaling after i.m. injection in the rat punch injury model (Figures 4E and 4F). Thus, our data strongly suggest the use of naked mRNA in a simple buffer formulation as a useful option for localized regenerative treatment of various tissues.

Our study also confirmed that the administration of engineered IGF-I mRNA in both rat muscle injury and rabbit spinal disc herniation models remained at the injection site. In the rat punch injury model, exposure assessment revealed that the mRNA was detected only in closer proximity to the injection site (1L and 2L segments, approximately 1 cm from injection site), confirming the limited spatial distribution of mRNA (no exposure in 3L and 4L; Figure 4C). In the rabbit spinal disc herniation model, each animal served as its own control by receiving vehicle solution in the L2/L3 disc, a sham procedure without injury in the L3/L4 disc, and engineered IGF-I mRNA in the L4/L5 disc. As the DHI data and histology outcomes differ for each disc, we presume no leakage of IGF-I mRNA into the neighboring discs. A similar observation was noted in diabetes patients who were treated with naked VEGFA mRNA (AZD8601) that increased VEGFA levels only at the injection site but did not enhance no systemic VEGFA levels.³⁷ In contrast to naked mRNA, LNP-formulated mRNA injected into the same tissue causes systemic exposure.⁵¹ Although we observed therapeutic effects of engineered IGF-I mRNA in two different disease models, our approach has limitations related to the mechanism of action of the mRNA modality. For example, the direct injection of IGF-I mRNA in the vertebral disc requires living cells at the injection site to translate the RNA into functional protein; thus, the proposed therapy may not work in patients with advanced spinal disc herniation and completely degenerated (black) discs but is implicated for use at an earlier stage of disease with higher regenerative capacity.⁷

In conclusion, the present study demonstrates feasibility of the local injection of engineered IGF-I mRNA formulated in simple buffer as therapy for muscle injury and spinal disc herniation. IGF-I mRNA treatment can further be envisioned for indications for which local i.m. administration to repair or regenerate tissue is warranted (e.g., into sphincter muscles in incontinent patients, joint or peripheral nerve injuries). Bringing IGF-I to expression locally using mRNA is believed to open up the possibility to fully use the regenerative potential of IGF-I in a more effective manner than previous attempts using rhIGF-I and modified or formulated versions thereof, and the proposed strategy can be applied for other diseases for which tissue regeneration is a potentially curative option.

MATERIALS AND METHODS

Construct design

The constructs encoding for pre-pro-IGF-I with either the natural SP (Cpd.1), or two heterologous SPs (Cpd.2 and Cpd.3) were gene synthesized in pMA vector backbone from GeneArt (www.thermofisher.com). The Cpd.1 IGF-I construct consisted of the natural SPs (pre-domain, 21 amino acids), the sequence encoding the human IGF-I pro-domain (27 amino acids), and the sequence encoding the full coding sequence of mature human IGF-I with 70 amino acids (Supplement data, Table S1). To enhance the secretion of mRNA-induced IGF-I out of the transfected cell, the natural IGF-I SP was exchanged by that of BDNF in Cpd.2, and Cpd.3 contained a SP from NTF-3. All the three constructs included the T7 promoter, unstructured UTRs (5' and 3'), a Kozak sequence, and a codon-optimized IGF-I open reading frame.

IVT

The transcription template from all the three constructs were generated by PCR using mRNA forward primer 5'-GCTGCAAGGCGATT AAGTTG-3' and mRNA reverse primer 5' U (2'OMe) U (2'OMe) U (2'OMe) T₍₁₁₇₎ CAGCTATGACCATGTTAATGCAG-3'. The reverse primer contained 120 nucleotide poly-T to include a poly-A tail into the mature mRNA. The mRNA was synthesized by *in vitro* transcription using T7 polymerase using MEGAscript T7 kit and were purified using the MEGAclean kit (www.thermofisher.com). All IVT mRNAs were quantified with nano-photometer and bio-analyzed for quality using the RNA6000 kit in Agilent 2100 Bio-analyzer (www.agilent.com).

Improvement of IGF-I secretion through SP optimization *in vitro*

HEK293 cells (CRL-1573; American Type Culture Collection [ATCC], Rockville, MD), Human hepatoma cell line (HepG2; catalog #85011430, European Collection of Authenticated Cell Cultures [ECACC]) and murine C2C12 cells (CRL-1772; ATCC) were maintained in DMEM (FG0445; Biochrome) supplemented with 10% (v/v) fetal bovine serum (FBS; www.biochrom.com), and penicillin-streptomycin-amphotericin B mixture (882087; -Biozym Scientific). HSkMCs (CC-2561; Lonza, Basel, Switzerland) were maintained in skeletal muscle cells growth medium (PromoCell) supplemented with penicillin-streptomycin-amphotericin B. In both DMEM and skeletal muscle cell growth medium,

the final concentration of antibiotic mixture was 0.25 µg/mL of amphotericin B, potassium penicillin (100 U/mL) streptomycin sulfate (100 µg/mL). Human Caucasian neuroblastoma IMR32 cells (catalog #86041809; ECACC) were maintained in Eagle's minimum essential medium (EMEM; catalog #1-31S01-I; BioConcept [www.bioconcept.ch]) supplemented with 10% (v/v) heat-inactivated FBS, L-glutamine (2 mM), and non-essential amino acids (NEAAs; 1×). Rat primary motoneurons were derived from spinal cords of 14 day gestational fetuses removed from euthanized pregnant female wild-type Wistar rats (Janvier Labs). The cells dissociated by trypsin/EDTA treatment and mechanical forced passages through the tip of a 10 mL pipette were maintained in a defined culture medium consisting of neurobasal medium containing 2% B27 supplement, 2 mmol/L glutamine, 2% penicillin-streptomycin, and 10 ng/mL BDNF. All cells were incubated at 37°C in a humidified atmosphere containing 5% CO₂. Forty-eight hours prior to transfection, HEK293 and C2C12 were plated at 20,000 cells/well, HepG2 cells were plated at 40,000 cells/well, and C2C12 and HSkMCs were plated 24 h prior to transfection at 80,000 cells/well seeding density in 96-well-microtiter plates. IMR32 cells were plated at 60,000 cells/well. After 11–12 days in culture, rat primary motoneurons were seeded at 20,000 cells/well. Thereafter, cells were transfected with varying concentrations depends on earlier mRNA optimization to specific cell line (HepG2, 300 ng; HEK293, 300 ng; C2C12, 300 ng; HSkMCs, 2000 ng; rat primary motor neurons, 300 ng) of three different IGF-I mRNAs (Cpd.1, Cpd.2, and Cpd.3) using Lipofectamine 2000 following the manufacturer's instructions (www.thermofisher.com). IMR32 cells were transfected with 300 ng of Cpd.1, Cpd.2, and Cpd.3 using JetMessenger (www.polyplus-transfection.com) following the manufacturer's instructions. A dose-response study was performed in HEK293 cells for endogenous IGF-I mRNA and Cpd.1 mRNA with doses of 0.02, 0.06, 0.2, 0.6, and 2 µg. Rat primary motoneurons were transfected using JetMessenger following the manufacturer's instructions (www.polyplus-transfection.com). After 5 h, the transfection complex was removed, plates were incubated for 24 h and cell culture supernatants were collected and analyzed for IGF-I expression by ELISA (E20; Mediagnost [www.mediagnost.de]).

Animal welfare compliance

All rodent animal experiments were performed following approval from the Institutional Animal Care and Use Committee of the Office of Animal Welfare Assurance at the University of Maryland School of Medicine and conformed to all Association for Assessment and Accreditation of Laboratory Animal Care guidelines. The rabbit disc herniation study was approved by the institutional ethics committee of AGINKO Research (authorization number 00391.01). This study was designed to use the fewest number of animals possible while being consistent with the objective of this study and the scientific needs and while taking into account all regulatory requirements. Procedures used in the study were designed to conform to accepted practices and to minimize or avoid causing pain, distress, or discomfort to the animals.

Mouse myotoxic injury model

For myotoxic injury model, male C57BL6/J mice 8–10 weeks old were purchased from Charles River Laboratories and housed at the study site (Myologica, Baltimore, MD). Mice were anesthetized with isoflurane and were injected i.m. with 0.04 mL of notexin (0.4 µg; Latoxan, Valence, France) into the right TA muscle; no adjustment was made on notexin dose relevant to animal body weight. The animals were observed for procedure-related pain, and upon requirement, appropriate anti-pain treatment was administered subsequently (buprenorphine 0.05–0.1 mg/kg every 12 h for 48 h after injection). The animals were monitored for proper healing and return of normal gait. To test the therapeutic efficacy of the mRNA encoding for endogenous human pre-pro-IGF-I (Cpd.1) in this model, mice were subjected to notexin-induced myotoxic injury in the TA, followed by injection with vehicle or 3, 10, or 30 µg Cpd.1, formulated in citrated saline buffer, i.m. at days 1 and 4 post-injury. Muscle function in the TA was measured at days 4, 7, 10, 14, 17, 21, and 28 post-injury using 305C muscle lever system (Aurora Scientific, Inc.). Optimal isometric twitch torque was determined by increasing frequency of stimulation (0.2 ms pulse, 500 ms train duration): 1, 10, 20, 40, 60, 80, 100, and 150 Hz, followed by a final stimulation at 1 Hz. Maximal peak isometric force was plotted. A subset of contralateral TAs were also assessed throughout the study. The schematic experimental design is shown in the [Table S2](#).

At the end of the study, the mice were euthanized via cervical dislocation, and both TA muscles were isolated, weighed, prepared for histology in optimal cutting temperature (OCT) and frozen in 2-methylbutane, and stored at –80°C. Histology analysis were performed to determine mean fiber CSA, regenerating fiber counts and muscle fiber typing using routine techniques. Detailed technical information on histology is provided in [Table S2](#). A second study was conducted to compare the muscle function recovery potential of Cpd.1 in a dose response to an mRNA coding for pre-pro-IGF-I with an optimized SP (BDNF pre-domain, Cpd.2) in the same notexin-induced myotoxic injury in the TA by applying mRNAs at 0.05, 0.15, 0.5, 1, 1.5, 3, 10, or 30 µg on days 1 and 4 post-injury.

Rat muscle punch injury model for PK/PD analysis

To test PK and PD properties of Cpd.2 mRNA, a punch biopsy model was established in adult male Sprague-Dawley rats (350–375 g, 10–15 weeks old; Myologica). The rat was anesthetized with isoflurane (~2%–3% or to effect) and the animal placed on a warmed (35°C) surgical table. The skin over the mid belly of the TA muscle was prepared by depilating the area (Nair Hair Remover for 45 s, followed by rinsing 3 times with water) and further prepped with three alternating scrubs of betadine and 70% ethyl alcohol to prevent seeding skin bacteria into the soft tissue. A small ~5 mm incision was performed in the skin and the muscle fascia to expose the muscle, and a 4 mm tissue punch biopsy was performed to full muscle depth. The biopsy was snap frozen and stored at –80°C until shipping. After ensuring that bleeding had stopped, two injections of 15 µL each containing 1, 10, or 30 µg Cpd.2 each was performed on either side of the punch injury. Rats were administered carprofen I.P. 1 mg/kg once a day for three days for pain relief. Animals were euthanized at 6, 24, 48, or 72 h

after administration ($n = 6$ per each time point). Additional vehicle treatment group with bunch biopsy was assigned at all time points ($n = 3$). Blood samples were collected in Qiagen RNAprotect Blood Tubes (www.qiagen.com) by cardiac puncture at time of termination. Immediately after exsanguination, the injected TA muscle was removed and several samples were then collected using a 3 mm tissue punch, starting distal from the injury and getting proximal to the location of the original punch biopsy (Figure 4A). Each sample was then flash frozen and a new punch made for each sample. Tools were wiped with an RNase decontaminant solution (RNase Zap; www.thermofisher.com) followed by RNase-free water between each animal collection to prevent RNA degradation by RNases. All tissue samples were stored at $\leq -70^{\circ}\text{C}$ until analysis.

qRT-PCR analysis

For the absolute quantification of IGF-I mRNA from injected muscle tissues, a qRT-PCR-based TaqMan assay was developed and validated (QPS LLC). Quantitation of exogenous IGF-I mRNA target sequence was performed by plotting the cycle threshold (Ct) value obtained from the test article on a regression line composed of standards of known concentration. The primers and probe in the TaqMan assay were designed to detect only exogenous IGF-I mRNA (Cpd.1, Cpd.2, and Cpd.3) as it binds to the codon-optimized sequence of the mRNA but not endogenous IGF-I RNA molecules. The specificity of this assay is verified by QPS. Total RNA was extracted from tissue using QIAasympyphony RNA Kit (www.qiagen.com), and qRT-PCR was performed using qScript XLT One-Step RT-qPCR ToughMix (www.quantabio.com) in the QuantStudio 7 Flex Real-Time PCR System (www.thermofisher.com). In order to confirm the activation of the muscle regeneration process after punch injury, a set of key myogenic biomarkers, including Pax7, MyoG, MYH3, MYH8, MyoD1, Myf5, and MYH4, were measured for their mRNA expression levels through relative quantification using Luna Universal One-Step RT-qPCR Kit (<https://international.neb.com>). The primer and probe details are provided in Table 1.

Protein analysis: IGF-I protein and pAKT

Muscle samples of 1R and 2R at all time points were processed for protein analysis. In brief, protease and phosphatase I and II were added to 1x PBS, and 150 μL PBS with Inhibitors distributed to each labeled bead bug column. Samples were thawed, washed using cold PBS, and cut into smaller pieces. A uniform amount of each sample was added to a labeled bead bug tube containing PBS with inhibitors (150 μL). Samples were loaded into the bead bug mixer and tissues minced for 180 s at 400 rpm. Samples were then removed and spun down to collect the macerate. To each sample 150 μL of 2x cell lysis buffer (EL-Lys; RayBiotech [<https://www.raybiotech.com/cell-tissue-lysis-buffer-item-j/>]) was added and incubated for 30 min at 4°C . Thereafter, samples were centrifuged at 4°C and 12,000 rpm for 25 min, and supernatants were collected. Protein analysis of human IGF-I was performed at RayBiotech using the RayBio Human IGF-I IQELISA Kit (catalog #IQH-IGF-I; <https://www.raybiotech.com/human-IGF-I-iqelisa-kit-en/>) according to the user manual. Protein analysis of pAKT was performed at RayBiotech using the RayBio Human, Mouse and

Table 1. Sequence details of primers and probes used in qRT-PCR analysis

Gene Name	Primer Sequence (5'-3')
IGF-I (TaqMan)	Forward: CGGTCTGAGGAGCCCTTCTAG
	Probe: CTGCTGCCGTAGCCTG
	Reverse: CGACAGAGGCTTCTACTTCAACAAG
Pax7	Forward: GTTCGGGAAGAAAGAGGACGAT
	Reverse: GGTTCCTGATTCCACGTCGAGCC
MyoG	Forward: TGGAGCTGTATGAAACATCCC
	Reverse: TGGACAATGCTCAGGGGTCCC
MYH3	Forward: CTCGCCAAGTCGGAGGCAAAGA
	Reverse: TCGCATCGCTCCTCGGCATCCA
MYH8	Forward: GGAGGACAAAGTCAACACCCTG
	Reverse: CCTCCAGTTTCTCTTGGCTCT
MYH4	For: AGAGCCAAGAGGAAACTGGAGG
	Reverse: TTCATCTCAATCTTGCTCTGC
Myf5	Forward: GGTAGAGAACTATTACAGCCTGC
	Reverse: GCAGTAGATGCTGTCAAAGCTAC
MyoD1	Forward: GCACTACAGCGCGACTCAGAC
	Reverse: TAGTAGGCGCGCTCGTAGCCAT
PPIA	Forward: GGCAAATGCTGGACCCAACACA
	Reverse: TGCTGGTCTTGCCATTCTGGA
IGF-I	Forward: GCAATGGGAAAAATCAGCAG
	Reverse: GAGGAGGACATGGTGTGCA

Rat Phospho-AKT (Ser473) and Total AKT ELISA Kit (catalog #PE-L-AKT-S473-T; <https://www.raybiotech.com/human-mouse-rat-phospho-akt-s473-and-total-akt-elisa/>) according to the user manual.

Rabbit model of intervertebral disc degeneration

To evaluate the safety and performance of Cpd.3 IGF-I mRNA, an intervertebral disc (IVD) degeneration model was established in adult males New Zealand white rabbits ($n = 8$; AGINKO Research). The IVD degeneration model was created according to a previously published method of the annulus puncture.⁵⁷ In brief, on day 0, a 22G spinal needle (22G \times 3.5 inches, 0.7 \times 90 mm) attached to a 10 mL syringe was inserted 3–4 cm ventral from the midline into the disc space under fluoroscopic control, held for 10 s, and rotated 180° before removal. Suction was applied by withdrawing through the 10 mL syringe to denucleate the IVD. The depth of the needle was controlled by a fluoroscope. Each rabbit had two discs punctured (L2/L3 and L4/L5). The non-punctured L3/L4 disc in between both served as control. This step is illustrated in Figures 6D and 6E. On days 30, 37, 44, and 51, each rabbit received 20 μL fluid of Cpd.3 administrated into the L4/L5 disc, and at the same times 20 μL of saline solution (0.9%) was injected into L2/L3 disc. The injections were done under X-ray control, using a 1 mL syringe and a 22G spinal needle. Body weight and X-ray analysis were measured on days 0, 30, 60, and 90. X-ray analysis was performed to quantify disc degeneration by measuring the DHI as previously described.⁵⁸ The rabbits' spines were X-Rayed and the vertebral body

of L2, L3, L4, and L5 and intervertebral space of L2/L3, L3/L4, and L4/L5 were measured using ImageJ software. Changes in the DHI of injected discs were normalized to the preinjected IVD height (day 0 values) and expressed as percentage DHI (%DHI). The calculation of DHI and %DHI is described in [Figure S7](#).

After day 90, animals were euthanized and spines collected, and the muscle and soft tissue were removed. After this step, the spines were cut with a saw and the IVD placed into cassettes for decalcification for 3 weeks. After the decalcification step, the rabbit spines were cut into 3 parts (L2/L3, L4/L5, and L3/L4), and each one of them was cut in half, giving two parts, A and B, which were embedded into paraffin. The paraffin-embedded blocks were sectioned (5 μ m) at 1 level. Six histological cuts were performed per level, slides were stained with toluidine blue and Masson's trichrome, and 3 slides were kept as reserve. Blind to the conditions, the pathologist analyzed histological sections for all rabbits. A scale based on 4 categories of degenerative changes with scores ranging from "normal disc" to "severely degenerated disc," spanning 12 points (3 points in each category), was used to assess IVD state. The scoring definition of IVD histology data provided in [Table S3](#).

Statistical analysis

Data were analyzed using Prism 8 (GraphPad Software, San Diego, CA). Data are presented as mean \pm SEM with three replicates. For the estimation of the IGF-I levels using ELISA in the standard or the sample, the mean absorbance value of the blank was subtracted from the mean absorbance of the standards or the samples. A standard curve was generated and plotted using a four parameters non-linear regression according to manufacturer's protocol. To determine the concentration of IGF-I in each sample the concentration was interpolated from the standard curve. The final protein concentration of the sample was calculated by multiplication with the dilution factor. Statistical analysis was carried out using Student's t test and one-way or two-way ANOVA as appropriate.

DATA AND CODE AVAILABILITY

All relevant data generated or analyzed during this study are included in this published article and its supplemental material files.

FUNDING

The work presented here was funded by Versameb AG.

SUPPLEMENTAL INFORMATION

Supplemental information can be found online at <https://doi.org/10.1016/j.omtn.2023.102055>.

ACKNOWLEDGMENTS

The authors would like to thank Mr. Pierre Mainil-Varlet (AGINKO Research AG) for performing disc herniation study.

AUTHOR CONTRIBUTIONS

F.M. and J.S.A. conceived and designed the experiments; P.B., C.B., S.Z., J.S.A., C.H., and R.K. performed the experiments; J.S.A., F.M.,

and K.P.Z. wrote the original draft of the manuscript; F.M., J.S.A., H.S., and P.H. analyzed the data; J.S.A., F.M., K.P.Z., P.H., H.S., A.H., A.T.S., I.K., and I.F. reviewed and edited the manuscript; J.S.A., F.M., and K.P.Z. provided supervision.

DECLARATION OF INTERESTS

Versameb AG is a privately held company focusing on discovering and developing innovative RNA-based drugs based in Basel, Switzerland. All authors affiliated with Versameb AG were employees during the course of this work and equity holders of Versameb.

REFERENCES

- Philippou, A., and Barton, E.R. (2014). Optimizing IGF-I for skeletal muscle therapeutics. *Growth Hormone IGF Res.* 24, 157–163. <https://doi.org/10.1016/j.ghir.2014.06.003>.
- Kletzl, H., Guenther, A., Höflich, A., Höflich, C., Frystyk, J., Staack, R.F., Schick, E., Wandel, C., Bleich, N., and Metzger, F. (2017). First-in-man study with a novel PEGylated recombinant human insulin-like growth factor-I. *Growth Hormone IGF Res.* 33, 9–16. <https://doi.org/10.1016/j.ghir.2017.01.001>.
- Ahmad, S.S., Ahmad, K., Lee, E.J., Lee, Y.H., and Choi, I. (2020). Implications of Insulin-Like Growth Factor-1 in Skeletal Muscle and Various Diseases. *Cells* 9. <https://doi.org/10.3390/cells9081773>.
- Vassilakos, G., and Barton, E.R. (2018). Insulin-Like Growth Factor I Regulation and Its Actions in Skeletal Muscle. *Compr. Physiol.* 9, 413–438. <https://doi.org/10.1002/cphy.c180010>.
- Yoshida, T., and Delafontaine, P. (2020). Mechanisms of IGF-1-Mediated Regulation of Skeletal Muscle Hypertrophy and Atrophy. *Cells* 9. <https://doi.org/10.3390/cells9091970>.
- Heron-Milhavet, L., Mamaeva, D., LeRoith, D., Lamb, N.J., and Fernandez, A. (2010). Impaired muscle regeneration and myoblast differentiation in mice with a muscle-specific KO of IGF-IR. *J. Cell. Physiol.* 225, 1–6. <https://doi.org/10.1002/jcp.22218>.
- Lin, H., Tian, S., Peng, Y., Wu, L., Xiao, Y., Qing, X., and Shao, Z. (2021). IGF Signaling in Intervertebral Disc Health and Disease. *Front. Cell Dev. Biol.* 9, 817099. <https://doi.org/10.3389/fcell.2021.817099>.
- Masuda, K., and An, H.S. (2004). Growth factors and the intervertebral disc. *Spine J.* 4, 330S–340S. <https://doi.org/10.1016/j.spinee.2004.07.028>.
- Beauverd, M., Mitchell, J.D., Wokke, J.H.J., and Borasio, G.D. (2012). Recombinant human insulin-like growth factor I (rhIGF-I) for the treatment of amyotrophic lateral sclerosis/motor neuron disease. *Cochrane Database Syst. Rev.* 11, CD002064. <https://doi.org/10.1002/14651858.CD002064.pub3>.
- Ostrowski, P.P., Barszczyk, A., Forstenpointner, J., Zheng, W., and Feng, Z.P. (2016). Meta-Analysis of Serum Insulin-Like Growth Factor 1 in Alzheimer's Disease. *PLoS One* 11, e0155733. <https://doi.org/10.1371/journal.pone.0155733>.
- Yamahara, K., Yamamoto, N., Kuwata, F., and Nakagawa, T. (2022). Neuroprotective role of insulin-like growth factor 1 in auditory and other nervous systems. *Histol. Histopathol.* 37, 609–619. <https://doi.org/10.14670/HH-18-437>.
- Cheetham, T.D., Connors, M., Clayton, K., Watts, A., and Dunger, D.B. (1997). The relationship between overnight GH levels and insulin concentrations in adolescents with insulin-dependent diabetes mellitus (IDDM) and the impact of recombinant human insulin-like growth factor I (rhIGF-I). *Clin. Endocrinol.* 46, 415–424. <https://doi.org/10.1046/j.1365-2265.1997.1320953.x>.
- Kemp, S.F. (2007). Mecasermin rinfabate. *Drugs Today* 43, 149–155. <https://doi.org/10.1358/dot.2007.43.3.1079876>.
- Metzger, F., Sajid, W., Saenger, S., Staudenmaier, C., van der Poel, C., Sobottka, B., Schuler, A., Sawitzky, M., Poirier, R., Tuerck, D., et al. (2011). Separation of fast from slow anabolism by site-specific PEGylation of insulin-like growth factor I (IGF-I). *J. Biol. Chem.* 286, 19501–19510. <https://doi.org/10.1074/jbc.M110.172189>.
- Martins, K.J.B., Gehrig, S.M., Naim, T., Saenger, S., Baum, D., Metzger, F., and Lynch, G.S. (2013). Intramuscular administration of PEGylated IGF-I improves skeletal

- muscle regeneration after myotoxic injury. *Growth Hormone IGF Res.* 23, 128–133. <https://doi.org/10.1016/j.ghir.2013.03.002>.
16. Huang, C.L., Leblond, A.L., Turner, E.C., Kumar, A.H., Martin, K., Whelan, D., O'Sullivan, D.M., and Caplice, N.M. (2015). Synthetic chemically modified mrna-based delivery of cytoprotective factor promotes early cardiomyocyte survival post-acute myocardial infarction. *Mol. Pharm.* 12, 991–996. <https://doi.org/10.1021/mp5006239>.
 17. Wu, H., Peng, Z., Xu, Y., Sheng, Z., Liu, Y., Liao, Y., Wang, Y., Wen, Y., Yi, J., Xie, C., et al. (2022). Engineered adipose-derived stem cells with IGF-1-modified mRNA ameliorates osteoarthritis development. *Stem Cell Res. Ther.* 13, 19. <https://doi.org/10.1186/s13287-021-02695-x>.
 18. Anderson, B.C., Christiansen, S.P., Grandt, S., Grange, R.W., and McLoon, L.K. (2006). Increased extraocular muscle strength with direct injection of insulin-like growth factor-I. *Invest. Ophthalmol. Vis. Sci.* 47, 2461–2467. <https://doi.org/10.1167/iovs.05-1416>.
 19. Nystrom, G., Pruznak, A., Huber, D., Frost, R.A., and Lang, C.H. (2009). Local insulin-like growth factor I prevents sepsis-induced muscle atrophy. *Metabolism* 58, 787–797. <https://doi.org/10.1016/j.metabol.2009.01.015>.
 20. Golombek, S., Pilz, M., Steinle, H., Kochba, E., Levin, Y., Lunter, D., Schlensak, C., Wendel, H.P., and Avci-Adali, M. (2018). Intradermal Delivery of Synthetic mRNA Using Hollow Microneedles for Efficient and Rapid Production of Exogenous Proteins in Skin. *Mol. Ther. Nucleic Acids* 11, 382–392. <https://doi.org/10.1016/j.omtn.2018.03.005>.
 21. Phua, K.K.L., Leong, K.W., and Nair, S.K. (2013). Transfection efficiency and transgene expression kinetics of mRNA delivered in naked and nanoparticle format. *J. Contr. Release* 166, 227–233. <https://doi.org/10.1016/j.jconrel.2012.12.029>.
 22. Sultana, N., Magadam, A., Hadas, Y., Kondrat, J., Singh, N., Youssef, E., Calderon, D., Chepurko, E., Dubois, N., Hajjar, R.J., and Zangi, L. (2017). Optimizing Cardiac Delivery of Modified mRNA. *Mol. Ther.* 25, 1306–1315. <https://doi.org/10.1016/j.ymthe.2017.03.016>.
 23. Tiwari, P.M., Vanover, D., Lindsay, K.E., Bawage, S.S., Kirschman, J.L., Bhosle, S., Lifland, A.W., Zurla, C., and Santangelo, P.J. (2018). Engineered mRNA-expressed antibodies prevent respiratory syncytial virus infection. *Nat. Commun.* 9, 3999. <https://doi.org/10.1038/s41467-018-06508-3>.
 24. Sahin, U., Karikó, K., and Türeci, Ö. (2014). mRNA-based therapeutics—developing a new class of drugs. *Nat. Rev. Drug Discov.* 13, 759–780. <https://doi.org/10.1038/nrd4278>.
 25. Owji, H., Nezafat, N., Negahdaripour, M., Hajiebrahimi, A., and Ghasemi, Y. (2018). A comprehensive review of signal peptides: Structure, roles, and applications. *Eur. J. Cell Biol.* 97, 422–441. <https://doi.org/10.1016/j.ejcb.2018.06.003>.
 26. Gutiérrez, J.M., and Ownby, C.L. (2003). Skeletal muscle degeneration induced by venom phospholipases A2: insights into the mechanisms of local and systemic myotoxicity. *Toxicon* 42, 915–931. <https://doi.org/10.1016/j.toxicon.2003.11.005>.
 27. Hardy, D., Besnard, A., Latil, M., Jouvion, G., Briand, D., Thépenier, C., Pascal, Q., Guguin, A., Gayraud-Morel, B., Cavallion, J.M., et al. (2016). Comparative Study of Injury Models for Studying Muscle Regeneration in Mice. *PLoS One* 11, e0147198. <https://doi.org/10.1371/journal.pone.0147198>.
 28. Plant, D.R., Colarossi, F.E., and Lynch, G.S. (2006). Notexin causes greater myotoxic damage and slower functional repair in mouse skeletal muscles than bupivacaine. *Muscle Nerve* 34, 577–585. <https://doi.org/10.1002/mus.20616>.
 29. Dayneka, N.L., Garg, V., and Jusko, W.J. (1993). Comparison of four basic models of indirect pharmacodynamic responses. *J. Pharmacokinet. Biopharm.* 21, 457–478. <https://doi.org/10.1007/BF01061691>.
 30. Ciciliot, S., and Schiaffino, S. (2010). Regeneration of mammalian skeletal muscle. Basic mechanisms and clinical implications. *Curr. Pharmaceut. Des.* 16, 906–914. <https://doi.org/10.2174/138161210790883453>.
 31. Fortier, L.A., Mohammed, H.O., Lust, G., and Nixon, A.J. (2002). Insulin-like growth factor-I enhances cell-based repair of articular cartilage. *J. Bone Joint Surg. Br.* 84, 276–288. <https://doi.org/10.1302/0301-620x.84b2.11167>.
 32. Gruber, H.E., Hoelscher, G.L., Ingram, J.A., Bethea, S., and Hanley, E.N. (2008). IGF-1 rescues human intervertebral annulus cells from in vitro stress-induced premature senescence. *Growth Factors* 26, 220–225. <https://doi.org/10.1080/08977190802273814>.
 33. Sobajima, S., Shimer, A.L., Chadderdon, R.C., Kompel, J.F., Kim, J.S., Gilbertson, L.G., and Kang, J.D. (2005). Quantitative analysis of gene expression in a rabbit model of intervertebral disc degeneration by real-time polymerase chain reaction. *Spine J.* 5, 14–23. <https://doi.org/10.1016/j.spinee.2004.05.251>.
 34. Antony, J.S., Dewerth, A., Haque, A., Handgretinger, R., and Kormann, M.S.D. (2015). Modified mRNA as a new therapeutic option for pediatric respiratory diseases and hemoglobinopathies. *Mol. Cell. Pediatr.* 2, 11. <https://doi.org/10.1186/s40348-015-0022-6>.
 35. Vavilis, T., Stamoula, E., Ainzoglou, A., Sachinidis, A., Lamprinou, M., Dardalas, I., and Vizirianakis, I.S. (2023). mRNA in the Context of Protein Replacement Therapy. *Pharmaceutics* 15, 166. <https://doi.org/10.3390/pharmaceutics15010166>.
 36. Anttila, V., Saraste, A., Knuuti, J., Hedman, M., Jaakkola, P., Laugwitz, K.L., Krane, M., Jeppsson, A., Sillanmäki, S., Rosenmeier, J., et al. (2023). Direct intramyocardial injection of VEGF mRNA in patients undergoing coronary artery bypass grafting. *Mol. Ther.* 31, 866–874. <https://doi.org/10.1016/j.ymthe.2022.11.017>.
 37. Gan, L.M., Lagerström-Fermér, M., Carlsson, L.G., Arfvidsson, C., Egnell, A.C., Rudvik, A., Kjaer, M., Collén, A., Thompson, J.D., Joyal, J., et al. (2019). Intradermal delivery of modified mRNA encoding VEGF-A in patients with type 2 diabetes. *Nat. Commun.* 10, 871. <https://doi.org/10.1038/s41467-019-08852-4>.
 38. Song, Y.H., Song, J.L., Delafontaine, P., and Godard, M.P. (2013). The therapeutic potential of IGF-I in skeletal muscle repair. *Trends Endocrinol. Metabol.* 24, 310–319. <https://doi.org/10.1016/j.tem.2013.03.004>.
 39. Güler-Gane, G., Kidd, S., Sridharan, S., Vaughan, T.J., Wilkinson, T.C.I., and Tigue, N.J. (2016). Overcoming the Refractory Expression of Secreted Recombinant Proteins in Mammalian Cells through Modification of the Signal Peptide and Adjacent Amino Acids. *PLoS One* 11, e0155340. <https://doi.org/10.1371/journal.pone.0155340>.
 40. Collén, A., Bergenhem, N., Carlsson, L., Chien, K.R., Hoge, S., Gan, L.M., and Fritsche-Danielson, R. (2022). VEGFA mRNA for regenerative treatment of heart failure. *Nat. Rev. Drug Discov.* 21, 79–80. <https://doi.org/10.1038/s41573-021-00355-6>.
 41. Karalaki, M., Fili, S., Philippou, A., and Koutsilieris, M. (2009). Muscle regeneration: cellular and molecular events. *In Vivo* 23, 779–796.
 42. Kiselyov, V.V., Versteyhe, S., Gauguin, L., and De Meyts, P. (2009). Harmonic oscillator model of the insulin and IGF1 receptors' allosteric binding and activation. *Mol. Syst. Biol.* 5, 243. <https://doi.org/10.1038/msb.2008.78>.
 43. De Meyts, P. (1994). The structural basis of insulin and insulin-like growth factor-I receptor binding and negative co-operativity, and its relevance to mitogenic versus metabolic signalling. *Diabetologia* 37, S135–S148. <https://doi.org/10.1007/BF00400837>.
 44. De Meyts, P., Ursø, B., Christoffersen, C.T., and Shymko, R.M. (1995). Mechanism of insulin and IGF-I receptor activation and signal transduction specificity. Receptor dimer cross-linking, bell-shaped curves, and sustained versus transient signaling. *Ann. N. Y. Acad. Sci.* 766, 388–401. <https://doi.org/10.1111/j.1749-6632.1995.tb26688.x>.
 45. De Meyts, P., Wallach, B., Christoffersen, C.T., Ursø, B., Grønskov, K., Latus, L.J., Yakushiji, F., Ilondo, M.M., and Shymko, R.M. (1994). The insulin-like growth factor-I receptor. Structure, ligand-binding mechanism and signal transduction. *Horm. Res.* 42, 152–169. <https://doi.org/10.1159/000184188>.
 46. Carlsson, L., Clarke, J.C., Yen, C., Gregoire, F., Albery, T., Billger, M., Egnell, A.C., Gan, L.M., Jennbacken, K., Johansson, E., et al. (2018). Biocompatible, Purified VEGF-A mRNA Improves Cardiac Function after Intracardiac Injection 1 Week Post-myocardial Infarction in Swine. *Mol. Ther. Methods Clin. Dev.* 9, 330–346. <https://doi.org/10.1016/j.omtm.2018.04.003>.
 47. Peletier, L.A., Gabriëlsson, J., and Haag, J.d. (2005). A dynamical systems analysis of the indirect response model with special emphasis on time to peak response. *J. Pharmacokinet. Pharmacodyn.* 32, 607–654. <https://doi.org/10.1007/s10928-005-0047-x>.
 48. Surinya, K.H., Forbes, B.E., Occhiodoro, F., Booker, G.W., Francis, G.L., Siddle, K., Wallace, J.C., and Cosgrove, L.J. (2008). An investigation of the ligand binding properties and negative cooperativity of soluble insulin-like growth factor receptors. *J. Biol. Chem.* 283, 5355–5363. <https://doi.org/10.1074/jbc.M707054200>.
 49. Urano, T., Narusawa, K., Shiraki, M., Usui, T., Sasaki, N., Hosoi, T., Ouchi, Y., Nakamura, T., and Inoue, S. (2008). Association of a single nucleotide polymorphism in the insulin-like growth factor-1 receptor gene with spinal disc degeneration in

- postmenopausal Japanese women. *Spine* 33, 1256–1261. <https://doi.org/10.1097/BRS.0b013e3181715304>.
50. Haque, A.A., Weinmann, P., Biswas, S., Handgretinger, R., Mezger, M., Kormann, M.S.D., and Antony, J.S. (2020). RNA ImmunoGenic Assay: A Method to Detect Immunogenicity of in vitro Transcribed mRNA in Human Whole Blood. *Bio. Protoc.* 10, e3850. <https://doi.org/10.21769/BioProtoc.3850>.
 51. Fertig, T.E., Chitoiu, L., Marta, D.S., Ionescu, V.S., Cismasiu, V.B., Radu, E., Angheluta, G., Dobre, M., Serbanescu, A., Hinescu, M.E., and Gherghiceanu, M. (2022). Vaccine mRNA Can Be Detected in Blood at 15 Days Post-Vaccination. *Biomedicines* 10, 1538. <https://doi.org/10.3390/biomedicines10071538>.
 52. Hotz, C., Wagenaar, T.R., Gieseke, F., Bangari, D.S., Callahan, M., Cao, H., Diekmann, J., Diken, M., Grunwitz, C., Hebert, A., et al. (2021). Local delivery of mRNA-encoded cytokines promotes antitumor immunity and tumor eradication across multiple preclinical tumor models. *Sci. Transl. Med.* 13, eabc7804. <https://doi.org/10.1126/scitranslmed.abc7804>.
 53. Chabanovska, O., Galow, A.M., David, R., and Lemcke, H. (2021). mRNA - A game changer in regenerative medicine, cell-based therapy and reprogramming strategies. *Adv. Drug Deliv. Rev.* 179, 114002. <https://doi.org/10.1016/j.addr.2021.114002>.
 54. Kormann, M.S.D., Hasenpusch, G., Aneja, M.K., Nica, G., Flemmer, A.W., Herber-Jonat, S., Huppmann, M., Mays, L.E., Illenyi, M., Schams, A., et al. (2011). Expression of therapeutic proteins after delivery of chemically modified mRNA in mice. *Nat. Biotechnol.* 29, 154–157. <https://doi.org/10.1038/nbt.1733>.
 55. Lindsay, K.E., Vanover, D., Thoresen, M., King, H., Xiao, P., Badial, P., Arainga, M., Park, S.B., Tiwari, P.M., Peck, H.E., et al. (2020). Aerosol Delivery of Synthetic mRNA to Vaginal Mucosa Leads to Durable Expression of Broadly Neutralizing Antibodies against HIV. *Mol. Ther.* 28, 805–819. <https://doi.org/10.1016/j.ymthe.2020.01.002>.
 56. Schlake, T., Thess, A., Fotin-Mleczek, M., and Kallen, K.J. (2012). Developing mRNA-vaccine technologies. *RNA Biol.* 9, 1319–1330. <https://doi.org/10.4161/rna.22269>.
 57. Watanabe, A., Mainil-Varlet, P., Decambon, A., Aschinger, C., and Schiavinato, A. (2019). Efficacy of HYADD(R)4-G single intra-discal injections in a rabbit model of intervertebral disc degeneration. *Bio Med. Mater. Eng.* 30, 403–417. <https://doi.org/10.3233/BME-191062>.
 58. Masuda, K., Aota, Y., Muehleman, C., Imai, Y., Okuma, M., Thonar, E.J., Andersson, G.B., and An, H.S. (2005). A novel rabbit model of mild, reproducible disc degeneration by an anulus needle puncture: correlation between the degree of disc injury and radiological and histological appearances of disc degeneration. *Spine* 30, 5–14. <https://doi.org/10.1097/01.brs.0000148152.04401.20>.